MIT Libraries | DSpace@MIT

MIT Open Access Articles

A strategy to couple the material point method (MPM) and smoothed particle hydrodynamics (SPH) computational techniques

The MIT Faculty has made this article openly available. ***Please share*** how this access benefits you. Your story matters.

Citation: Raymond, Samuel J., Bruce Jones, and John R. Williams. "A Strategy to Couple the Material Point Method (MPM) and Smoothed Particle Hydrodynamics (SPH) Computational Techniques." Computational Particle Mechanics 5, no. 1 (December 10, 2016): 49–58.

As Published: http://dx.doi.org/10.1007/s40571-016-0149-9

Publisher: Springer International Publishing

Persistent URL: http://hdl.handle.net/1721.1/116233

Version: Author's final manuscript: final author's manuscript post peer review, without publisher's formatting or copy editing

Terms of use: Creative Commons Attribution-Noncommercial-Share Alike

Massachusetts Institute of Technology

Computational Particle Mechanics manuscript No.
(will be inserted by the editor)

A strategy to couple the Material Point Method (MPM) and Smoothed Particle Hydrodynamics (SPH) computational techniques

Samuel J. Raymond · Bruce Jones · John R. Williams

Received: date / Accepted: date

Abstract A strategy is introduced to allow coupling of the Material Point Method (MPM) and Smoothed Particle Hydrodynamics (SPH) for numerical simulations. This new strategy partitions the domain into SPH and MPM regions, particles carry all state variables and as such no special treatment is required for the transition between regions. The aim of this work is to derive and validate the coupling methodology between MPM and SPH. Such coupling allows for general boundary conditions to be used in an SPH simulation without further augmentation. Additionally, as SPH is a purely particle method and MPM is a combination of particles and a mesh, this coupling also permits a smooth transition from particle methods to mesh methods. Where further coupling to mesh methods could in future provide an effective farfield boundary treatment for the SPH method. The coupling technique is introduced and described alongside a number of simulations in 1-D and 2-D to validate and contextualize the potential of using these two methods in a single simulation. The strategy shown here is capable of fully coupling the two methods without any complicated algorithms to transform information from one method to another.

Keywords Meshfree · Coupling Technique · Boundary Conditions · Material Point Method · Smoothed Particle Hydrodynamics

1 Introduction

In the field of solid mechanics simulation meshless methods such as Smoothed Particle Hydrodynamics (SPH), and the Material Point Method (MPM), are being increasingly applied as an alternative to more traditional mesh based methods [1–4]. This is motivated by the fact that such methods are able to consider large deformations and discontinuities. The SPH method itself was originally developed to simulate astrophysics of gas dynamics in the late 1970's, it has now been used in a wide number of scientific fields including solid mechanics [5; 6] and geomechanics [7; 8], to thermal [9], fluid [10; 11], and even biophysical simulations [12].

Despite it's wide adoption, boundary conditions in SPH are notoriously difficult to generalize. This is essentially due to the manner in which the method is derived (See section 2). By definition, boundaries in SPH are "smoothed" making it difficult to place exact boundary conditions. Despite this, significant progress and varied success has been achieved by researchers in the field [7; 13]. An alternative solution to the issue of deficient boundaries would be to couple SPH to another numerical method which could be used instead when applying boundary conditions. Coupling numerical methods to utilize mutual distinctive advantages has been done in the past to simulate a wide range of physical processes [14–16]. SPH specifically has been coupled to a number of methods including the Discrete Element Method (DEM), and the Finite Element Method [14; 16–19]. This paper introduces a strategy to couple SPH to the Material Point Method (MPM). MPM is a meshfree method that utilizes material points and a background mesh to discretize the computational domain. With its use of both Lagrangian particles (as in SPH) and an Eulerian spatial grid (as in FEM), MPM has the potential to be an ideal candidate to couple with SPH and allow for better boundary representations. More details about MPM are given in section 3. Following introduction of the methods and coupling strategy, the coupled model is validated against a number of 1D and 2D test cases. The aim of this paper is to show a proof of concept for the coupling of SPH and MPM.

Samuel J. Raymond
Computational Science and Engineering
Civil and Environmental Engineering
Massachusetts Institute of Technology
E-mail: sjr@mit.edu

2 Smoothed Particle Hydrodynamics

In SPH a body is discretized into a number of particles. These particles are ascribed state variables such as mass, velocity, volume, pressures, stresses, to describe the material completely. As a Lagrangian method, SPH particles move with the body and deform according to the equations of motion. These equations typically derive from a Lagrangian function that desribes the physics involved. This allows SPH to have excellent conservation properties, as well as making the inclusion of extra physics a matter of altering the systems governing Lagrangian.

There is no background mesh in SPH, and particles are free to move and become disordered. Determination of gradient values is achieved by interpolation via a weighting function, commonly referred to as the SPH kernel. Each particle uses this function to gather information from neighbouring particles and by doing so, interacts with the surrounding particles. To develop the SPH kernel, the following mathematical identity for describing a function is presented.

$$A(\boldsymbol{x}) = \int_{\Omega} A(\boldsymbol{x}')\delta(\boldsymbol{x}' - \boldsymbol{x})d\boldsymbol{x} \tag{2.1}$$

where A is a vector function of the position vector $\boldsymbol{x}$, Ω is the volume of the integral containing the point $\boldsymbol{x}$, and $\delta(\boldsymbol{x}' - \boldsymbol{x})$ is the Dirac delta function. This equation expresses the vector function as an infinite sum of infinitesimals, an integral. The kernel function,$W(\boldsymbol{x}_a - \boldsymbol{x}_b, h)$, can be thought of as a smoothed delta function, but retaining certain convergence requirements and properties that ensure mathematical consistency. Additionally, instead of an integral, since each particle has an associated volume, the integral is replaced with a summation.

$$A(\boldsymbol{x}_a) = \sum_{b \in \Lambda_a} A_b \frac{m_b}{\rho_b} W(\boldsymbol{x}_a - \boldsymbol{x}_b, h) \tag{2.2}$$

with m_b the mass of particle b, and ρ_b the density of particle b. The parameter h used in the kernel is referred to as the smoothing length and is the radius of the kernel. Essentially this value acts as the resolution parameter of the SPH simulation. The value Λ, represents the domain of influence that the particle has. Typically this includes particles that are separated by less than a distance of h.Using the kernel approximation of 2.1, a derivative can also be defined.The gradient of the function A at the position of particle 'a' is evaluated by taking the derivative of the smoothing kernel.

$$\nabla A(\boldsymbol{x}_a) = \sum_{b \in \Lambda_a} A_b \frac{m_b}{\rho_b} \nabla_a W(\boldsymbol{x}_a - \boldsymbol{x}_b, h) \tag{2.3}$$

this feature of the smoothing kernel approximation of the function allows gradient quantities to be easily evaluated during a simulation as the smoothing kernel functions are known a-priori. Second derivatives can also be formed by first derivatives using Taylor expansions in a manner similarly used in Finite Difference methods. In practice, equation 2.3 is replaced and an alternative form used.

$$\nabla A(\boldsymbol{x}_a) = \sum_{b \in \Lambda_a} (A_b - A_a) \frac{m_b}{\rho_b} \nabla_a W(\boldsymbol{x}_a - \boldsymbol{x}_b, h) \tag{2.4}$$

this form of the derivate was found by Libersky*et al.*[20] to be more accurate and possessed better conservation properties. Using equations 2.2 and 2.4 and a suitable Lagrangian, the equations of motion for a given problem can be recast from their differential form to a discrete SPH form.

2.1 SPH approximation of governing equations

In order to solve problems dealing with continuum mechanics, SPH uses the conservation of mass, momenta, and energy laws to build the governing equations for a simulation. While in SPH the mass of a particle is fixed, the evolution of the density (and volume) is calculated using the SPH approximation of the continuity equation.

$$\frac{D\rho_a}{Dt} = \sum_{b \in \Lambda_a} m_b(\boldsymbol{v}_a - \boldsymbol{v}_b)\nabla_a W_{ab} \tag{2.5}$$

this is the material, or complete derivative, where ρ_a is the density of particle 'a' with velocity component, $\boldsymbol{v}_a$, m_b is the mass of the neighbour particle 'b' with velocity component $\boldsymbol{v}_b$, and $W_{ab} = W(\boldsymbol{x}_a - \boldsymbol{x}_b, h)$. For shorthand in the following equations, the subscript "v_{ab}" referrers to $v_a - v_b$. In this work, the following approximation of the momentum equation is used as per Gray and Monaghan [5].

$$\frac{D\boldsymbol{v}_a}{Dt} = \sum_{b\in\Lambda_a} m_b \left(\frac{\boldsymbol{\sigma}_a}{\rho_a^2} + \frac{\boldsymbol{\sigma}_b}{\rho_b^2} + \Pi_{ab} \right) \nabla_a W_{ab} \tag{2.6}$$

where, $\boldsymbol{\sigma_a}$ is the stress tensor of particle a, and Π_{ab} is the artificial viscosity, which is included to resolve any non-physical oscillation in the solution. The form of the artificial viscosity is the same in the work as used by Cleary in [21].

$$\Pi_{ab} = \begin{cases} \frac{-\alpha c_0 \eta_{ab} + \beta \eta_{ab}^2}{\bar{\rho}_{ab}} & \boldsymbol{v}_{ab} \cdot \boldsymbol{x}_{ab} < 0 \\ 0 & \boldsymbol{v}_{ab} \cdot \boldsymbol{x}_{ab} \geq 0, \end{cases} \tag{2.7}$$

where

$$\eta_{ab} = \frac{h_{ab} \boldsymbol{v}_{ab} \cdot \boldsymbol{x}_{ab}}{|r_{ab}|^2} \tag{2.8}$$

c_0 denotes the speed of sound of the material. To calculate the stress rate from the generalized Hooke's law, the strain rate tensor is approximated into the SPH form.

$$\dot{\boldsymbol{\varepsilon}}_a = \frac{1}{2} \left[\sum_{b\in\Lambda_a} \frac{m_b}{\rho_b} \boldsymbol{v}_{ba} \otimes \nabla_a W_{ab} + \left(\sum_{b\in\Lambda_a} \frac{m_b}{\rho_b} \boldsymbol{v}_{ba} \otimes \nabla_a W_{ab} \right)^{\mathsf{T}} \right] \tag{2.9}$$

To close the set of equations a constitutive model is introduced to transform the strains into stresses. For this work a simple elastic, small strains approach is followed.

Together, equations 2.5 - 2.9 and a suitable constitutive model allow the simulations of essentially any material behaviour in continuum mechanics. This is why SPH has transformed form a method handling astrophysical problems to one that can be used to model Newtonian fluids, non-Newtonian fluids, solids, fracturing materials, magnetohydrodynamics, as well as models that involve a combination of different physics.

3 The Material Point Method

The Material Point Method (MPM) discretizes a body in a similar manner to SPH. A geometry is divided into small mass elements, Fig. 1, referred to as material points, and assigned all the variables required to describe the state of the material: stress, strain, position, velocity, mass, etc.

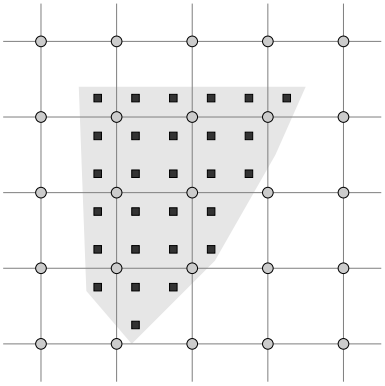

Fig. 1: A body discretized using material points and the surrounding mesh nodes.

Where this method differs from SPH is that these particles are then embedded in a background mesh that uses the same nodal shape functions found in FEM. Instead of the kernel function used on each SPH particle, during a time-step, information is transmitted from the material points to the nodes. Equations of motion are solved on the nodes, and the updated variables are sent to the material points in order to update their state variables. Once the material points have been updated, the grid is reset back to its original position, or updated for some specific purpose if the user so desires. MPM was largely developed in the Los Alamos National Labs[3] in the second half of the last century. It is an extension to the PIC/FLIP methods developed by Harlow and his colleagues from the

1950's [22]. PIC was developed in response to the motivation to model highly distorted fluid flow. This method was eventually extended to model solids by Sulsky et.al [23] in the mid 1990's. Today MPM has been applied in a number of fields including geomechanics [4; 24; 25], manufacturing [26; 27], sea ice dynamics [28; 29], and many more. A key advantage of MPM is that since the grid is reset at the end of each timestep, mesh tangling and distortions that can plague a typical Lagrangian FEM code under large deformation is entirely avoided [3; 23; 30]. Additionally, since MPM, like FEM, can be derived from the weak form of the variational principal, boundary conditions can be represented exactly on surfaces of nodes or material points [3]. This differs from SPH where boundaries are smoothed and cannot be exactly enforced without special treatments.

The MPM Timestep

The basic algorithm for an MPM time-step begins with extrapolating the mass, momenta, and stresses to the grid nodes so that the internal force equation can be formed. Extrapolation is made possible by use of nodal shape functions, $N_i(x)$, such that for node i the relevant shape function is:

$$N_i(x) = \begin{cases} 0 & x - x_i \geq -L, \\ 1 + \frac{(x-x_i)}{L} & -L < x - x_i \leq 0, \\ 1 - \frac{(x-x_i)}{L} & 0 < x - x_i \leq L, \\ 0 & L < x - x_i \end{cases} \tag{3.1}$$

with L being the cell-size of the MPM grid cell. The above 1-D formula can be extended to 3-D elements by simple multiplication: $N_i(x, y, z) = N_i(x)N_i(y)N_i(z)$. To extrapolate the required quantities to solve the equations of motion, the mass, momenta and internal forces are ascribed to grid as presented in general MPM literature (for example see [31]).

$$M_i = \sum^{N_p} m_p N_{ip} \tag{3.2}$$

$$M_i v_i = \sum^{N_p} m_p v_p N_{ip} \tag{3.3}$$

$$f_i^{int} = -\sum^{Np} \boldsymbol{\sigma}_p G_{ip} V_p \qquad (G_{ip} \equiv \nabla N_{ip}) \tag{3.4}$$

$$f_i^{ext} = \sum^{Np} m_p \boldsymbol{b} N_{ip} \tag{3.5}$$

In the above equations, M_i and m_p refer to the nodal and material point masses, respectively, N_{ip} and G_{ip} are the shape and gradient shape functions of node i with respect to material point p, v_i and v_p are the nodal and material point velocities respectively, f_i^{int} and f_i^{ext} are the internal and external nodal forces respectively, $\boldsymbol{\sigma}_p$ is the stress tensor for material point p ,V_p is the volume of material point p and $\boldsymbol{b}$ is a body force, such as gravity, that acts as an external force. Using the quantities from (3.2 - 3.5), Newton's second law of motion can be stated and the new acceleration for the current time step evaluated.

$$M_i a_i = f_i^{int} + f_i^{ext} \tag{3.6}$$

The acceleration of node i, a_i, can now be found and the grid velocity, v_i can be updated to v_i^* using the computational timestep Δt:

$$v_i^* = v_i + a_i \Delta t \tag{3.7}$$

In theory the grid positions would be updated too, however in practice this step is rarely explicitly performed and the grid is reset instead.

Now that the grid is in its updated state, the material points must be updated. Nodal acceleration and velocity gradients are sent to the material points to update their kinematic and constitutive variables. This process requires a reverse operation to the extrapolation performed at the beginning of the timestep. Instead of all the material points contributing to the relevant nodes, the nodes contribute to all material points within their vicinity. In a typical simulation the number of material points is larger than the number of nodes resulting in non-square matrices for

node-material point relationships [3; 27]. This prevents, in a general simulation, the inversion of a "shape function matrix" and requires a summation procedure instead of the contributing nodes.

$$v_p^* = v_p + \sum^{Ni} a_i \Delta t \tag{3.8}$$

$$x_p^* = x_p + v_p \Delta t \tag{3.9}$$

In equation 3.9, the material point position, x_p, is updated to a new position x_p^* using the material point velocity. In some instances it is better to use the updated grid velocity, or a contribution of each. More details of this can be found in [32].

To update the constitutive variables, for small strain theory, the velocity gradient, ∇v is used:

$$\varepsilon_p^* = \varepsilon_p + \frac{\Delta t}{2} \sum^{Ni} [v_i G_{ip} + G_{ip} v_i] \tag{3.10}$$

Using the strain, stresses can be updated using any constitutive law. In this work the generalized Hooke's law is used for all simulations.

$$\sigma_{ij} = \lambda \varepsilon_{ii} \delta ij + 2G\varepsilon_{ij} \tag{3.11}$$

The material constants λ and G are Lame's constants and δ_{ij} is the Dirac delta function. This material model can also include plasticity and other internal variable updates such as temperature and concentration.

Once the material point state variables have all been updated to the current values, the grid no longer carries any required information to describe the material and can be reset for the next time-step.

One modification to the above was implemented in this work. The Generalized Interpolated Material Point (GIMP) formulation for the shape function was used. This augmentation to "classical MPM" smooths, slightly, the shape function such that there is some overlap of the shape function domains. This method still preserves the partition of unity in the same manner as SPH, it just requires that the modified shape function be integrated. More details of this modification are found in [33–35].

4 Coupling Strategy

In the last section MPM was outlined as a way of particle information to be transfered to a background grid and back again. For SPH, as the method only consists of particles, a coupling between MPM and SPH would allow SPH to communicate with the nodes of MPM if they were within the domain of the nodal shape functions. This then provides a neat and simple manner in which to couple these two methods. Essentially the domain is discretized as shown in Fig. 2.

The two sets of domains, MPM and SPH are used to discretize the entire spatial domain. These domain may, but are not assumed to contain SPH particles or material points during the simulation. Prior to the addition of particles, the SPH region is essentially just empty space whereas the MPM region is filled with a background mesh, as would be found in a regular MPM simulation. As per the desired geometry, particles are then placed in the domain and are assigned a particle type. SPH particles are included in the MPM integration if they are within a cell's width of the grid. Similarly, material points are treated as SPH particles if the are within the domain of influence of these SPH particles that reside in the transition region. The transition region is set to be one cell width as this removes any incomplete nodal functions for the MPM summations and ensures partition of unity is maintained. For the tests in this paper the domain is discretized with an outer MPM grid and the inner space filled with an SPH domain, but this is only chosen for simplicity and clarity. A simulation could consist of regions of SPH domains and MPM domains, depending on the users requirements. The simplicity of this coupling is made possible due to the way in which the physical material is described by the particles in both methods. Apart from the solving of the equations of motion, and the expression of derivative values, both SPH and MPM describe the state of the material at a given time-step by a collection of Lagrangian particles. This allows the coupling to be a case of 'which integration scheme should each particle use to get updated?'. The MPM and SPH particles are solved in the time loop in their usual forms, separately, while the particles in the transition zone contribute to each integration phase, their assigned type controls which integration scheme is used for their update. To ensure a compatible spatial resolution, the smoothing length of the SPH particles is equal to the cell width of the MPM grid. This ensures that the shape functions used in both schemes are compatible. Using this method also means that no special interpolation functions are required for consistency across the two domains. SPH particles will "see" data points regardless of their type being material points or SPH particles, and the same argument holds for MPM nodes.

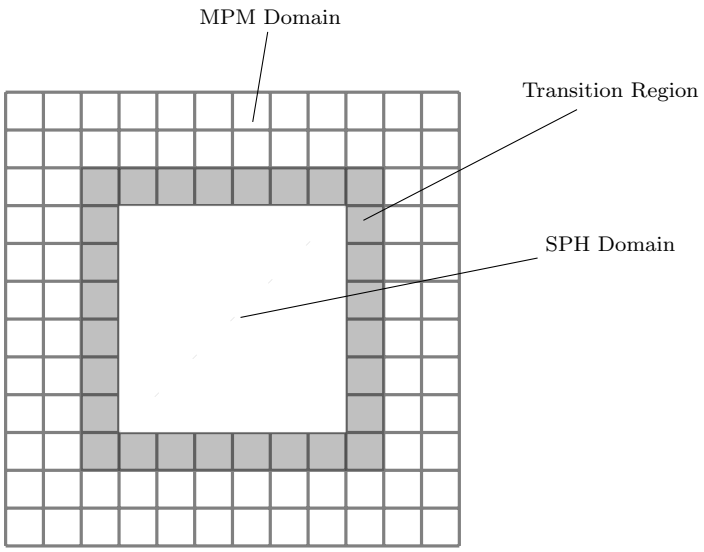

Fig. 2: Schematic of SPH-MPM geometry showing the different regions discretised as either MPM, SPH of transitional regions.

5 1-D Validation Tests

To evaluate the behavior and accuracy of the proposed coupling strategy a coupled MPM and SPH code was written in MATLAB and performed a number of tests to show the coupling strategy in practice.

5.1 Conservation and Reversibility

The first test consists of a prescribed initial velocity condition of the form:

$$v(x,0) = 0.01\ c_{speed}\ sin(10\pi x) \tag{5.1}$$

where c_{speed} is the sound speed of the material. After 500 time steps, the velocities of all the particles (and material points) are reversed and the integration continues for another 500 steps. This was applied to the problem schematic shown in Fig. 3. The results were then compared with the analytical results of the negative of the initial velocity condition. This test was proposed by Monaghan in [36] and is a good test of a codes conservation properties as well as the reversibility of the discretized equations of motion. A second order predictor-corrector integrator was used for all three codes and the simulation parameters used are shown in Table.1.

The final energy profile is shown in Fig. 4 and the velocity profile is shown in Fig. 5. When plotting velocity profile the background grid is depicted to show the extent of the computational domain, only during the calculation of gradients are they physically relevant, all permanent information is stored in the material points and SPH particles. The results are in excellent agreement with the analytical solution. These results show that the proposed coupling technique both conserves energy correctly and is fully reversible (constitutive model allowing).

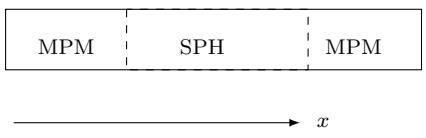

Fig. 3: Schematic of a 1D test of the coupled MPM-SPH model where an initial velocity is assigned to each point in the bar at t=0.

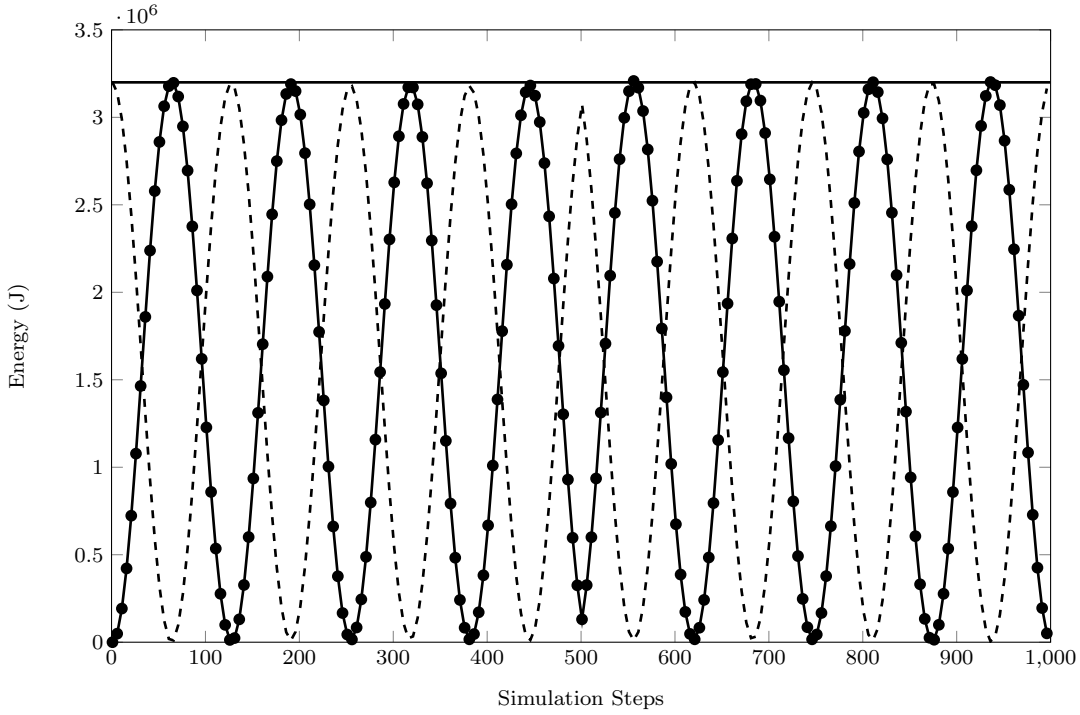

Fig. 4: Energy profile for the couple MPM-SPH simulation showing total energy (—), strain energy (–•–), and kinetic energy(- -).

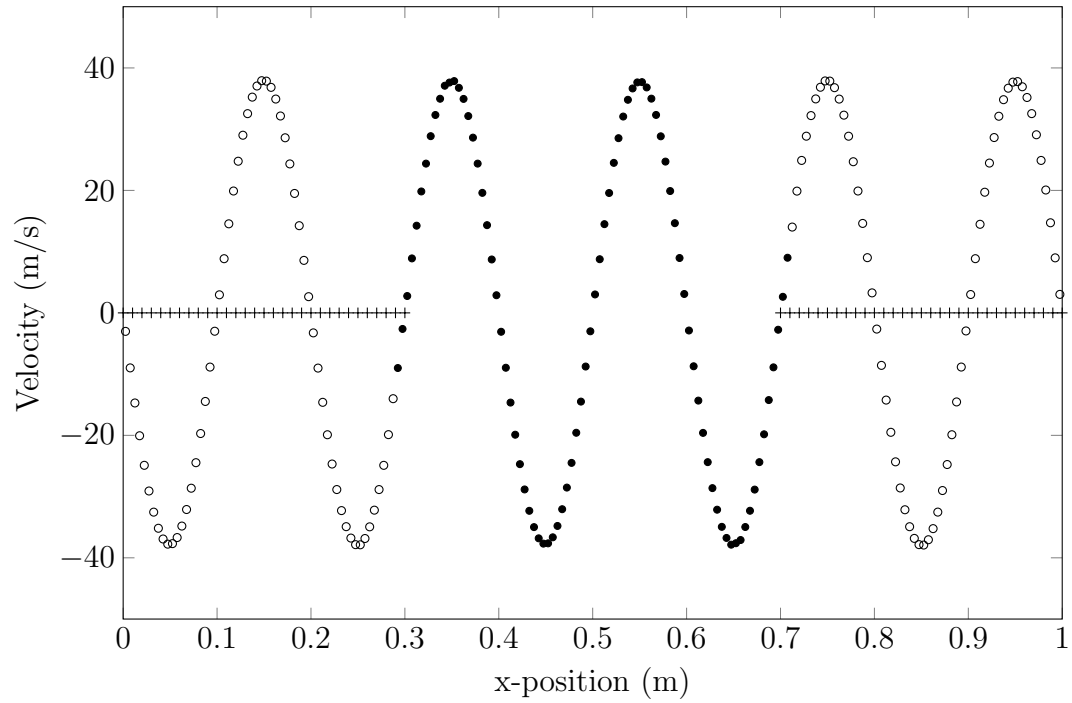

Fig. 5: Final velocity profile for the coupled MPM-SPH velocity simulation. (+) Background grid nodes, (○), and (•) SPH Particles.

Simulation Parameter	Value
Density, ρ	$8790 \frac{kg}{m^3}$
Young's Modulus, E	128GPa
Poisson's Ratio, ν	0.3
Cell-size (for MPM grid)	0.1m
Particle Separation (SPH and MPM)	0.05m
Courant Factor	0.1

Table 1: Simulation parameters of Copper used in the 1-D tests of the coupled MPM-SPH code tests.

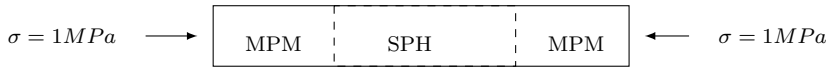

Fig. 6: Schematic of a 1D compression of a bar using the coupled MPM-SPH model.

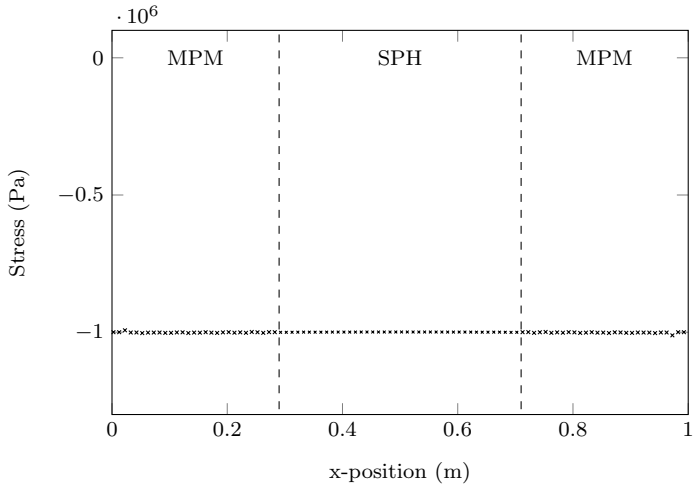

Fig. 7: Final stress profile for the coupled MPM-SPH simulation.

5.2 Application of Boundary Conditions

As mentioned earlier, applying boundary conditions in SPH often requires a variety of additional algorithms. In MPM, however, due to the derivation from the weak form of the equations of motion, exact boundaries can be represented on the mesh nodes and material points. These boundary conditions can be in the form of any traditional quantities: velocity, stress, thermal, etc. They can also be applied in a mixed form in MPM, for example velocity conditions can be placed on the mesh nodes and stress boundary conditions on the surface particles. This gives MPM flexibility over traditional mesh based techniques as well. For this test a stress value was assigned to the two opposite sides of the material. Aschematic of the problem is shown in Fig. 6 The stress was ramped initially and then held at a value.

Since the boundaries are placed in the MPM domain and the stress waves move internally to the SPH particles, the system responds as expected and the exact stress state is produced. Fig. 7 shows this final stress state. Analytically, the static strain value for a material with these properties would have a strain value of $\epsilon_{static} = -7.8125 \times 10^{-6}$. This compares to the value of $\epsilon_{coupledMPM-SPH} = -7.8938 \times 10^{-6}$, and an error of approximately 1%.

These results highlight that one of the motivations of this coupled approach, to ensure exact boundaries in an SPH simulation, can be achieved when applying stress boundary conditions. It also shows that this method is capable of transmitting all necessary information between the MPM nodes, material points and SPH particles.

6 2D Sample Simulations

A number of common solid mechanics tests were performed in 2D to determine the behavior of this coupling strategy in 2D mechanics problems. Two cases are presented here. The first being an extension of the compressed boundaries in 1D, a biaxially loaded square piece of material is loaded to an equilibrium state. Secondly, a plate with a hole

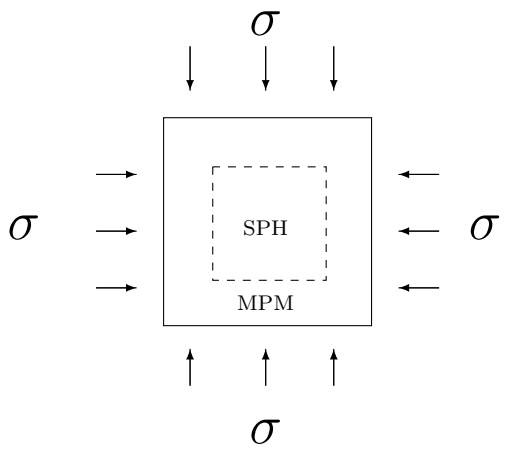

Fig. 8: 2D schematic of the biaxial compressive loading for the coupled MPM-SPH model.

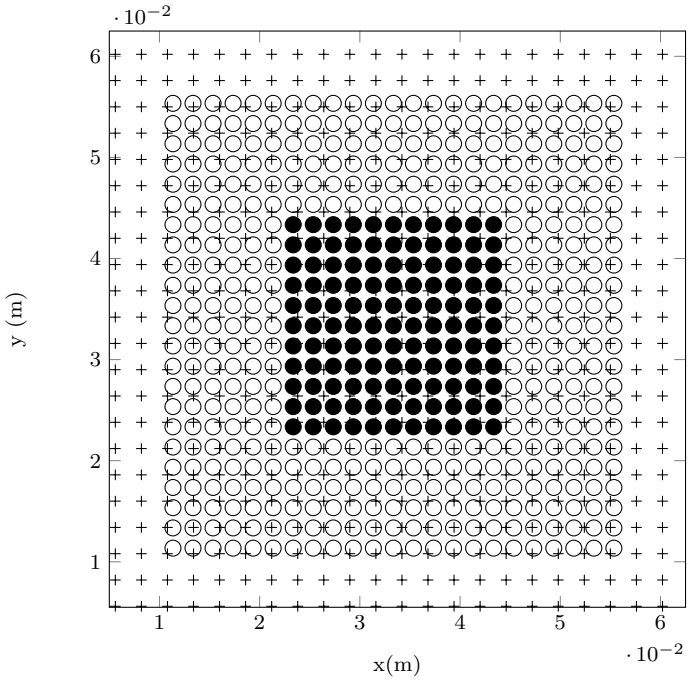

Fig. 9: Initial discretization of Material Points , and SPH particles for the biaxial loading test. (+) Background grid nodes, (○), and (●) SPH Particles.

is uniaxially loaded to produce a stress concentration. These examples are designed to test different aspects of the coupling behavior and shed more insight into the benefits of using these two methods side by side.

6.1 Biaxial Compression

A 2D plate is discretized as in Fig. 9. The plate is then subjected to a biaxial compression, by applying compressive stresses to the first two layers of particles along each boundary of the plate (in this case MPM particles). The applied stress is ramped to a constant value of 1MPa. Fig 10 shows the stresses along the horizontal center line of the material at the end of the simulation. The boundary value of 1MPa is well established across the SPH and MPM regions and the material is in a stable stress state.

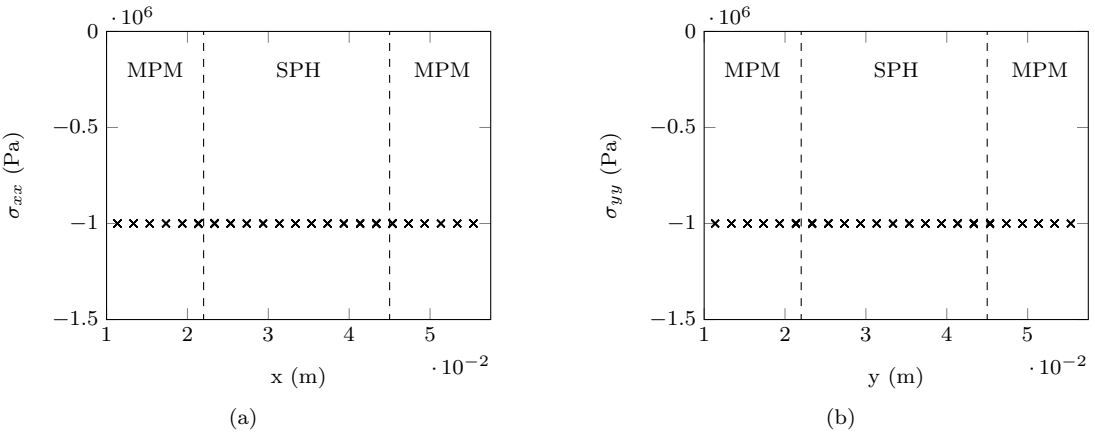

Fig. 10: Stress plots for the biaxially loaded plate. (a) σ_{xx} values along the horizontal centerline and (b) σ_{yy} values through the vertical centerline of the plate.

While these results are reasonably coarse, they highlight the potential for MPM to play a role in far-field boundary conditions and allowing SPH to model smaller scale internal features. Further investigation into the use of this arrangement is currently ongoing.

6.2 Hole in a uniaxially loaded plate

To test the smoothness of the coupling in regions of high stress gradients, a 2D plate containing a hole was discretized as in Fig. 11. The top and bottom two layers of particles were assigned a constant velocity of 1mm/s so as to produce a tensile load in the material. A schematic of the problem is shown in Fig. 12.

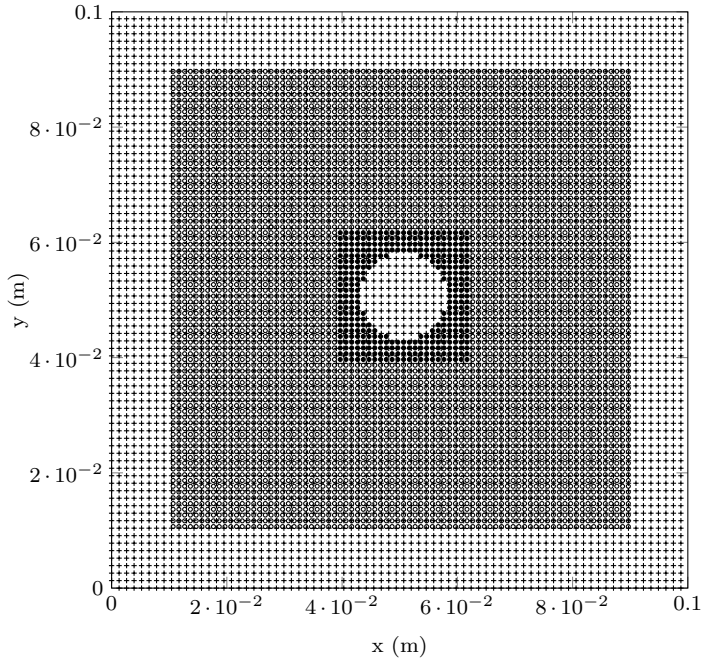

Fig. 11: Discretization of Material Points and SPH particles during the axially loaded hole in a plate test. (+) Background grid nodes, (∘), and (•) SPH Particles.

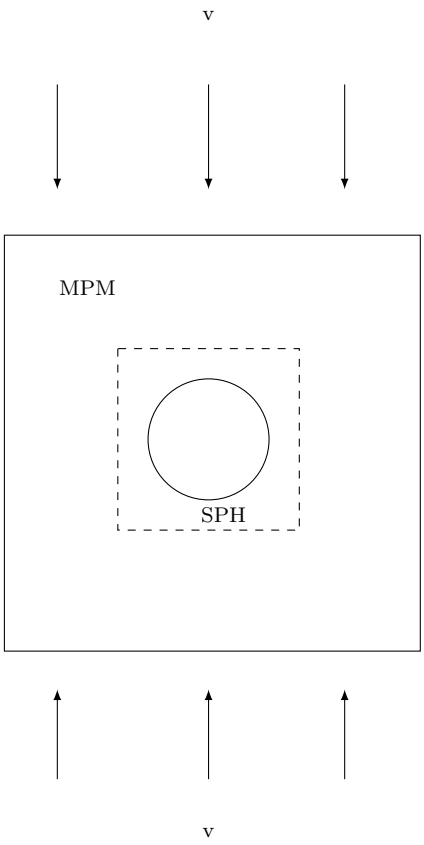

Fig. 12: 2D schematic of a plate with a hole under uniaxial loading simulated by the coupled MPM-SPH model.

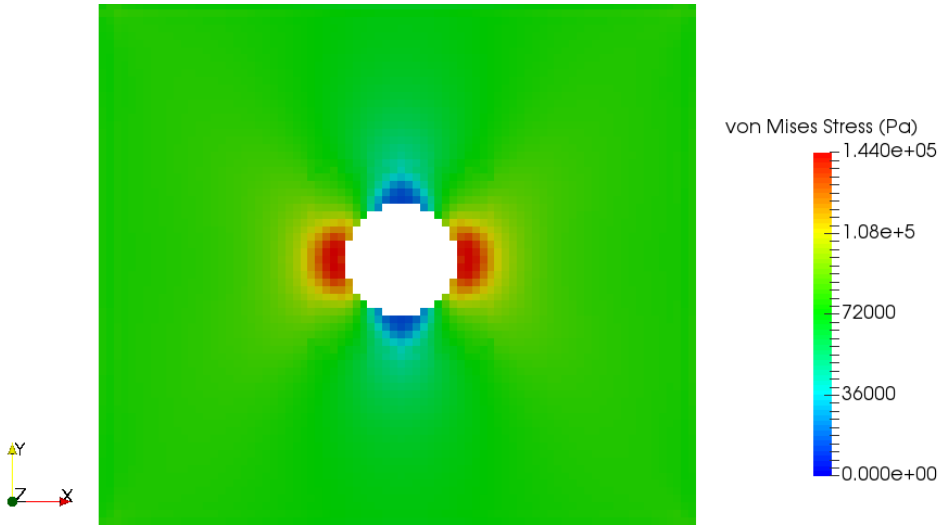

Fig. 13: von Mises stress field of the material during loading.

To better resolve the stress concentration about the hole the resolution for this simulation was increased and the von Mises stresses were calculated for Fig. 13. As expected there is a large stress concentration around the hole, contour lines also show the stress gradients.

It is also apparent that the transition from SPH to MPM creates no noticeable disturbance in the stress field. Fig. 14 shows the comparison of the stresses along the horizontal mid line simulated and predicted by theory. While the high stress gradient area is well reproduced, there are some oscillations further away from the stress concentration. This is most likely due to the limited extent of the material and the transient response of the

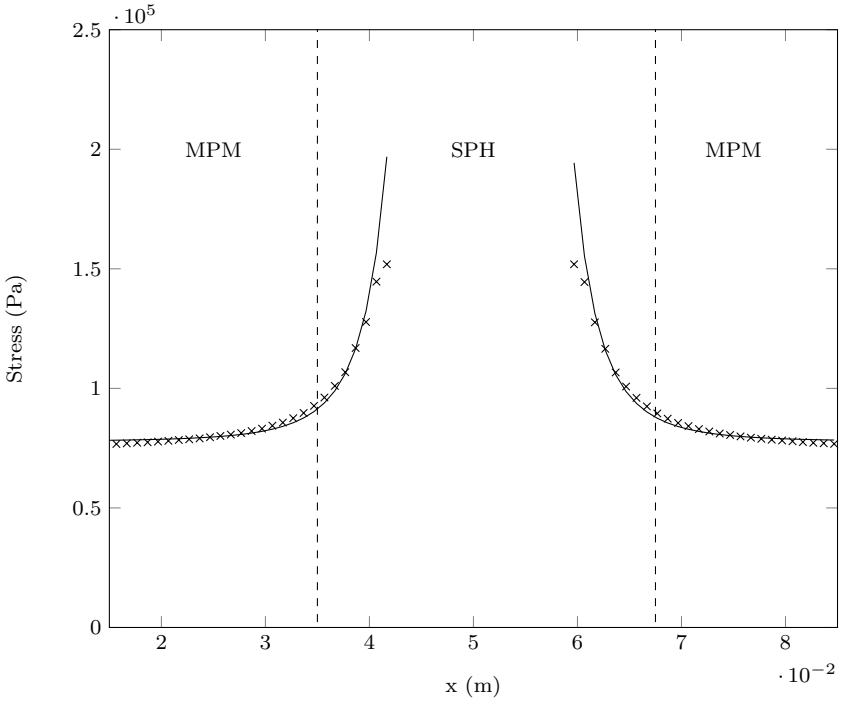

Fig. 14: Comparison of the equivalent stresses along the horizontal center line from the simulation (crosses) and the analytical solution(line).

material under this loading. These results imply that this coupling could be useful for large scale, high resolution problems with stress concentrations and far field boundary conditions.

7 Conclusion and Recommendations

In this paper a new coupling technique was proposed that allows simulations to be run using Smoothed Particle Hydrodynamics (SPH) and the Material Point Method (MPM). Using the compatible nature of the particles used to describe the materials in each method, a simple coupling based on position relative to each domain was used to couple the two integration methods. As boundary conditions arise naturally from the derivation of MPM but are generally difficult in SPH, using MPM to establish boundary conditions and propagate the information to the interior SPH particles yielded successful results. Test simulations in 1D, involving velocity and stress boundary conditions assigned to the surfaces of a material, show expected and stable behavior of the material. The success of the test simulations promote further investigation into the applicability of this coupling for more complex simulations. 2-D simulations of typical solid mechanics cases were run with the coupling of MPM and SPH showing several areas of potential benefit. It is also possible that this coupling could be used to apply spatially varying resolution of a region of large deformation in a concentrated place but with far-field effects. These and other applications will be the focus of further research.

Acknowledgements

The authors would like to thank the Abu Dhabi National Oil Company (ADNOC) for its scientific and financial support.

References

1. P. W. Cleary, M. Prakash, and J. Ha. Novel applications of smoothed particle hydrodynamics (SPH) in metal forming. *J. Mater. Process. Technol.*, 177(1-3):41–48, 2006.
2. P. W. Cleary, G. Savage, J. Ha, and M. Prakash. Flow analysis and validation of numerical modelling for a thin walled high pressure die casting using SPH. *Comput. Part. Mech.*, 1(3):229–243, 2014.
3. D. Sulsky, Z. Chen, and H. L. Schreyer. A particle method for history-dependent materials. *Comput. Methods Appl. Mech. Eng.*, 118:179–196, 1994.
4. S. Raymond, Y.E Aimene, J Nairn, and A Ouenes. Coupled Fluid-Solid Geomechanical Modeling of Multiple Hydraulic Fractures Interacting with Natural Fractures and the Resulting Proppant Modeling Proppant Distribution in the Presence of Natural Fractures using the Material Point Method (MPM). In *SPE Unconv. Resour. Conf.*, 2015.
5. J. P. Gray, J. J. Monaghan, and R. P. Swift. SPH elastic dynamics. *Comput. Methods Appl. Mech. Eng.*, 190(49-50):6641–6662, 2001.
6. W. Benz and E. Asphaug. Simulations of brittle solids using smooth particle hydrodynamics. *Comput. Phys. Commun.*, 87:253–265, 1995.
7. T. Douillet-grellier, R. Pramanik, K. Pan, A. Albaiz, B. D. Jones, and J. R. Williams. Development of stress boundary conditions in Smoothed Particle Hydrodynamics (SPH) for the modeling of solids deformation. *Comput. Part. Mech.*, pages 1–28, 2016.
8. S. Raymond, V. Lemiale, R. Ibrahim, and R. Lau. A meshfree study of the KalthoffWinkler experiment in 3D at room and low temperatures under dynamic loading using viscoplastic modelling. *Eng. Anal. Bound. Elem.*, 42:20–25, may 2014.
9. R. Das and P. W. Cleary. Effect of rock shapes on brittle fracture using Smoothed Particle Hydrodynamics. *Theor. Appl. Fract. Mech.*, 53(1):47–60, 2010.
10. Joseph J. Monaghan. Smoothed particle hydrodynamics. *Reports Prog. Phys.*, 68(8):1703–1759, 2005.
11. J. B. Kajtar and J. J. Monaghan. On the dynamics of swimming linked bodies. *Eur. J. Mech. B/Fluids*, 29(5):377–386, 2010.
12. P. W. Cleary, M. D. Sinnott, B. Hari, S. Bakalis, and S. M. Harrison. *Modelling food digestion.* Elsevier Ltd., 2015.
13. D. Violeau. *Fluid Mechanics and the SPH Method.* Oxford Press, 2012.
14. R Canelas, RML Ferreira, AJC Crespo, and JM Dominguez. A generalized SPH-DEM discretization for the modelling of complex multiphasic free surface flows. *Proc. 8th Int. SPHERIC Work.*, (June 4-6):6, 2013.
15. Y. Chuzel-Marmot, R. Ortiz, and A. Combescure. Three dimensional SPH-FEM gluing for simulation of fast impacts on concrete slabs. *Comput. Struct.*, 89(23-24):2484–2494, 2011.
16. P. W. Cleary. Prediction of coupled particle and fluid flows using DEM and SPH. *Miner. Eng.*, 73:85–99, 2015.

17. J. W. Fernandez, P. W. Cleary, M. D. Sinnott, and R. D. Morrison. Using SPH one-way coupled to DEM to model wet industrial banana screens. *Miner. Eng.*, 24(8):741–753, 2011.
18. Dean Hu, Ting Long, Yihua Xiao, Xu Han, and Yuantong Gu. Fluid-structure interaction analysis by coupled FE-SPH model based on a novel searching algorithm. *Comput. Methods Appl. Mech. Eng.*, 276:266–286, 2014.
19. Yrjo Jun Huang and Ole Jorgen Nydal. Coupling of discrete-element method and smoothed particle hydrodynamics for liquid-solid flows. *Theor. Appl. Mech. Lett.*, 2:012002, 2012.
20. Larry D. Libersky, Albert G. Petschek, Theodore C. Carney, Jim R. Hipp, and Firooz a. Allahdadi. High Strain Lagrangian Hydrodynamics, 1993.
21. P. W. Cleary. Elastoplastic deformation during projectile-wall collision. *Appl. Math. Model.*, 34(2):266–283, 2010.
22. F. H. Harlow and A. A. Amsden. A numerical fluid dynamics calculation method for all flow speeds. *J. Comput. Phys.*, 8(2):197–213, 1971.
23. D. Sulsky, S. Zhou, and H. L. Schreyer. Application of a particle-in-cell method to solid mechanics. *Comput. Phys. Commun.*, 87:236–252, 1995.
24. K. Abe, K. Soga, and S. Bandara. Material Point Method for Coupled Hydromechanical Problems. *J. Geotech. . . .*, pages 1–16, 2013.
25. K. Abe and K Konagai. Numerical simulation of a series of flume tests with dry and wet sands by using depth averaged material point method. In *Geomech. from Micro to Macro*, pages 971–976, 2015.
26. V. Lemiale, J. Nairn, and A. Hurmane. Material Point Method Simulation of Equal Channel Angular Pressing Involving Large Plastic Strain and Contact Through Sharp Corners. *C. - Comput. Model. Eng. Sci.*, 70(1):41–66, 2010.
27. D. Sulsky and A. Kaul. Implicit dynamics in the material-point method. *Comput. Methods Appl. Mech. Eng.*, 193(12-14):1137–1170, 2004.
28. D. Sulsky, H. L. Schreyer, K. Peterson, R. Kwok, and M. Coon. Using the material-point method to model sea ice dynamics. *J. Geophys. Res. Ocean.*, 112(August 2006):1–18, 2007.
29. D. Sulsky and K. Peterson. Toward a new elastic-decohesive model of Arctic sea ice. *Phys. D Nonlinear Phenom.*, 240(20):1674–1683, 2011.
30. J. Nairn. Material point method calculations with explicit cracks. *C. - Comput. Model. Eng. Sci.*, 4(6):649–663, 2003.
31. S.G. Bardenhagen, J.U. J. U. Brackbill, and D. Sulsky. The material-point method for granular materials. *Comput. Methods Appl. Mech. Eng.*, 187(99):529–541, 2000.
32. J. A Nairn. Numerical Modeling of Orthogonal Cutting : Application to Woodworking with a Bench Plane. pages 1–17, 2015.
33. S. G. Bardenhagen and E. M. Kober. The Generalized Interpolation Material Point Method. *C. - Comput. Model. Eng. Sci.*, 5(6):477–495, 2004.
34. A. Sadeghirad, R. Brannon, and J. Burghardt. A convected particle domain interpolation technique to extend applicability of the material point method for problems involving massive deformations. *Int. J. Numer. Methods Eng.*, 86(March):1435–1456, 2011.
35. A. Sadeghirad, Rebecca B., and J. E. Guilkey. Second-order convected particle domain interpolation (CPDI2) with enrichment for weak discontinuities at material interfaces. *Int. J. Numer. Methods Eng.*, 95(July):928–952, 2013.
36. J. J. Monaghan. Smoothed particle hydrodynamics. *Reports Prog. Phys.*, 68(8):1703, 2005.